Scientific Research Publishing

Journal of Geoscience and Environment Protection, 2023, 11, 79-118
https://www.scirp.org/journal/gep
ISSN Online: 2327-4344
ISSN Print: 2327-4336

Implications on Gravity Anomaly Measurements Associated with Different Lithologies in Turkana South Subcounty

Daniel Mogaka Nyaberi

Department of Environmental Earth Sciences, University of Eldoret, Uasin Gishu, Kenya
Email: nyaberimogaka@gmail.com

How to cite this paper: Nyaberi, D. M. (2023). Implications on Gravity Anomaly Measurements Associated with Different Lithologies in Turkana South Subcounty. *Journal of Geoscience and Environment Protection, 11,* 79-118.
https://doi.org/10.4236/gep.2023.111006

Received: December 7, 2022
Accepted: January 27, 2023
Published: January 30, 2023

Abstract

The use of gravity data has demonstrated capability for monitoring lithological changes on a large scale as a consequence of differentiating basement and sedimentary of buried valleys. Gravity anomalies are associated with lateral contrasts in density and therefore deformation by faulting or folding will be manifested if accompanied by lateral density changes, otherwise, the vice versa is true. The study's objective is to evaluate the effectiveness of gravity method in establishing different lithologies in an area. The study has revealed that regional anomaly gravity map presents high anomalies in the Northern region in the NW-SE trend and low anomalies in the southern trend in NW-SE, while the residual anomaly gravity map shows different trends for the low and high gravity anomalies. The gravity anomalies are well interpreted in line with the lithologies of the study area rather than the deformation of the same lithologies. There are observed high values of gravity anomaly values (ranging from −880.2 to −501.2 g.u.) where there are eolian unconsolidated rocks overlying the basement compared to low gravity anomaly values (ranging from −1338.9 to −1088.7 g.u.) where the andesites, trachytes and phonolites overly the basement. The different regional gravity anomalies relate well with different rock densities in the study area along the line profile for radially averaged power spectrum. The gravity highs are noted in the eastern point and are associated with andesites, trachytes, basalts and igneous rocks, while the gravity lows are associated with sandstone, greywacke, arkose, and eolian unconsolidated rock. The utilization of the information from the Power spectrum analysis demonstrates that the depth to the deepest basement rock is 12.8 km which is in the eastern flank, while the shallowest to the basement of 1.1 km to the western flank.

Keywords

Regional Gravity Anomalies, Power Spectrum Analysis, Density Contrasts,

Lithologies

1. Introduction

There subsist variations on the Earth materials' densities and the gravity technique measurements by yields deviations in the measured gravity field help pick where the differences in densities of subsurface rocks exist (Hakim, 2018). Gravity technique helps manifest the subsurface geologic structures (Balsubramanian, 2007) and has the capability of detecting the structural trends including mapping fractures and intrusions, determining the binding interfaces of bedrock, therefore becoming dominant method in geophysical surveys. Gravity application is greatly applied in investigating geological structures, ascertaining existence of geothermal reservoirs, detecting volcanic activity and hydrothermal movement beneath volcanoes, examination of CO_2 movement, locating active faults associated with earthquakes and detection of confined cavities (Hakim, 2018). The gravity method helps determine the configuration for the bedrock surface over an area of recent sediment cover (Idris et al., 2015), show the relationship between deeply buried basin and (Handayani et al., 2018) and find mineral resources and groundwater in sedimentary terrain (Balsubramanian, 2007; Chandler, 1994). Residual gravity anomalies' application in detection of the trends of the faults is tested in study areas by distinguishing between high and low gravity anomalies and the downthrown of faults towards low anomalies (Sultan et al., 2015).

The research deals with the southern part of Turkana County considering data from the gravity survey carried out from 1955 to 1975 (**Figure 1**). The objective of the study is to use the gravity data to advance geological interpretation in the region, especially looking at the subsurface structure of the basement and the relation of gravity in relation to known geology of the area.

2. Geology

The geology of Turkana South Subcounty (**Figure 2**) encompasses the basement (The Neoproterozoic belt), the tertiary volcanics and the quaternary sediments with similarities across border in eastern Uganda, and counties of West Pokot, Baringo, Samburu and area and Marsabit. The present-day basin has its origins in Pliocene tectonic developments. The Subcounty is traversed by the extensive of the modern rift, with subsidence making room for more than one kilometer of Plio-Pleistocene (Feibel, 2011). It is within this structure and deep basins exists manifestations of prospects of oil and gas deposits within sedimentary.

The metamorphic basement in the Turkana South Subcounty mainly of crystalline nature formed as part of the Mozambique Belt during a Neoproterozoic to Cambrian age mountain-building episode (Schlöter, 1997). The lithologies in the basement encompass schists, gneisses and marbles that originate from metamorphism of sandstones, sediments-grits, limestones and shales due from

heat, pressure or through impregnation by permeating subsurface fluids. Igneous rock formations are comparatively rare and are made up of granitic masses and dykes, and sills of epidioritic and amphibolitic nature resultant from originally dolerite material or associated rocks, and more or less ultrabasic lithologic formations. Some of the formations are seemingly younger as compared to the metamorphism that affected the sedimentary host rocks, though all are undoubtedly of Precambrian in age.

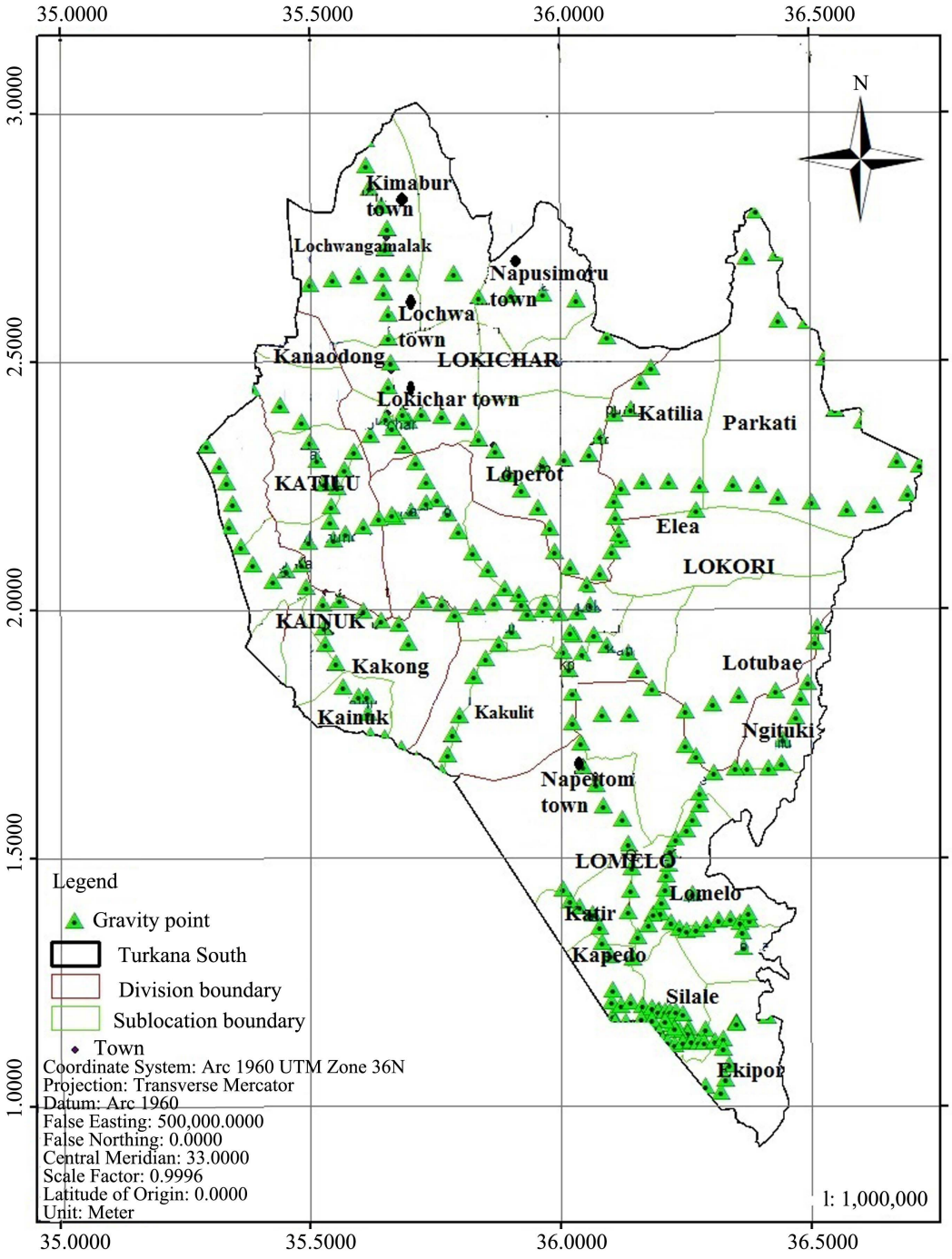

Figure 1. Gravity data locations of in study area.

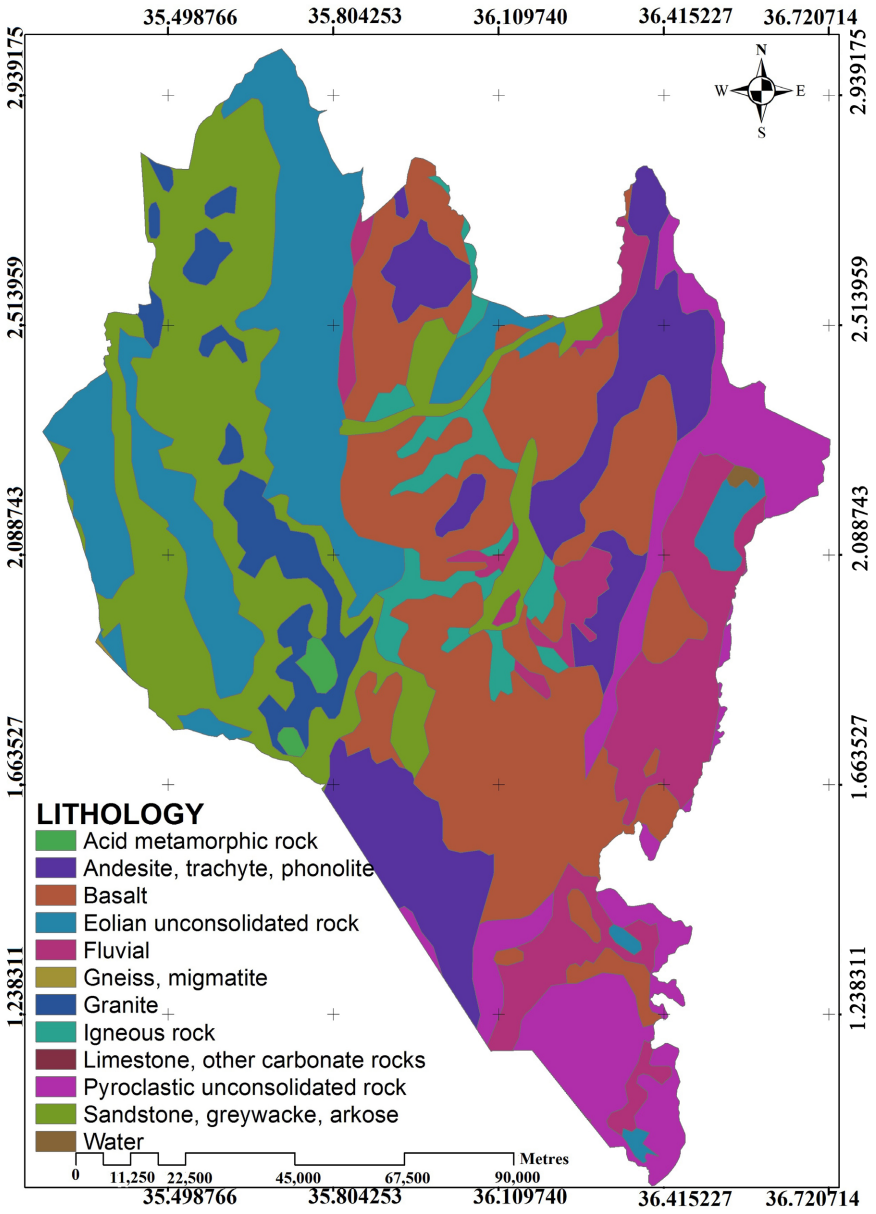

Figure 2. The geological map of Turkana South Subcounty.

The older sediments accumulated within components of the Central African Rift System or in isolated depositional basins (Feibel, 2011). These sedimentary strata offer a limited opening unto understanding earlier stages in the geological history of the region as revealed from some outcroping, faulting, or uncertain relationships to broader depositional systems, which preserve vital paleontological records and are important openings towards deciphering evolutionary patterns across Africa (Feibel, 2011).

The Late Eocene to Miocene volcanics dominated by extensive basalts volcanic rocks cover a large proportion of the study area, and attain considerable thickness. These are the oldest volcanic rocks which are generally fine-grained basalts which overlie the Turkana Grits. This volcanic series of basalts tend to

weather fairly rapidly by mechanical breakdown on joints and fractures, which reduce much of the mass of the exposed rock to small boulders and cobble which in their turn suffer surface weathering and alteration. For this reason, the topography of outcrops of the lower basalts is generally a series of low rolling hills. The volcanics shape much of the landscape, and are significant contributors to sediment flux and solutes. Volcanic raw materials are also the dominant sources used in manufacture of most of the Turkana basin's archaeological record (Roche et al., 2004). Volcanism is of a "cyclic" nature, and six cycles of plateau basalt eruption followed by salic, usually trachyte central volcano activity are recognised (Truckle, 1977). The dominant mechanism of deformation is noted particularly from the morphology of multi-centred plateau basalt formations and dykes and their relationship to progressive easterly tilting (Truckle, 1977).

There is an emerging understanding of the link between extensional pulses and magmatic episodes especially modern magmatism located within the Turkana Depression and its relationship with the distribution of extensional strain and find that the magmas are derived from sub-lithospheric sources equivalent to magmatism in the more mature sectors of the rift (Rooney et al., 2022).

These Quaternary are sediments of the Lake Turkana basin and according to Walsh and Dodson (1969) the formation comprises a sequence of lacustrine deposits of Pleistocene age and whose accumulation and formation has continued through to the recent period. Evidently, the geology of Turkana South Subcounty is to a larger way affected by geological structures which are cross cutting the metamorphic and igneous formations in the region (**Figure 3**).

3. Materials and Methods of Research

3.1. Gravity Method Theory and Application

Gravity method is referred to as a potential field method because the measurements involve a function of the potential of the observed field of force, i.e. terrestrial gravity, at the observation site (Hinze et al., 2013). The gravity method operates on basis that depends on two laws derived by Newton, namely, the Universal Law of gravitation, and the Second Law of Motion. Using Kepler's empirical third Law (Equation (1)) which relates the period (T) and the semi-major axis (a) of the orbit of the satellite to the mass (M) of the parent body, Newton deduced that the force of attraction between a planet and the Sun varied with the "quantities of solid matter that they contain" (i.e., their masses) and with the inverse square of the distance between them (Lowrie, 2007) whose application to two particles or point masses m and M separated by a distance r gives relationship for the gravitational attraction F exerted by M on m (Equation (2)).

$$GM = \frac{4\pi^2}{T^2} a^3 \tag{1}$$

$$F = -G\frac{mM}{r^2}\bar{r} \tag{2}$$

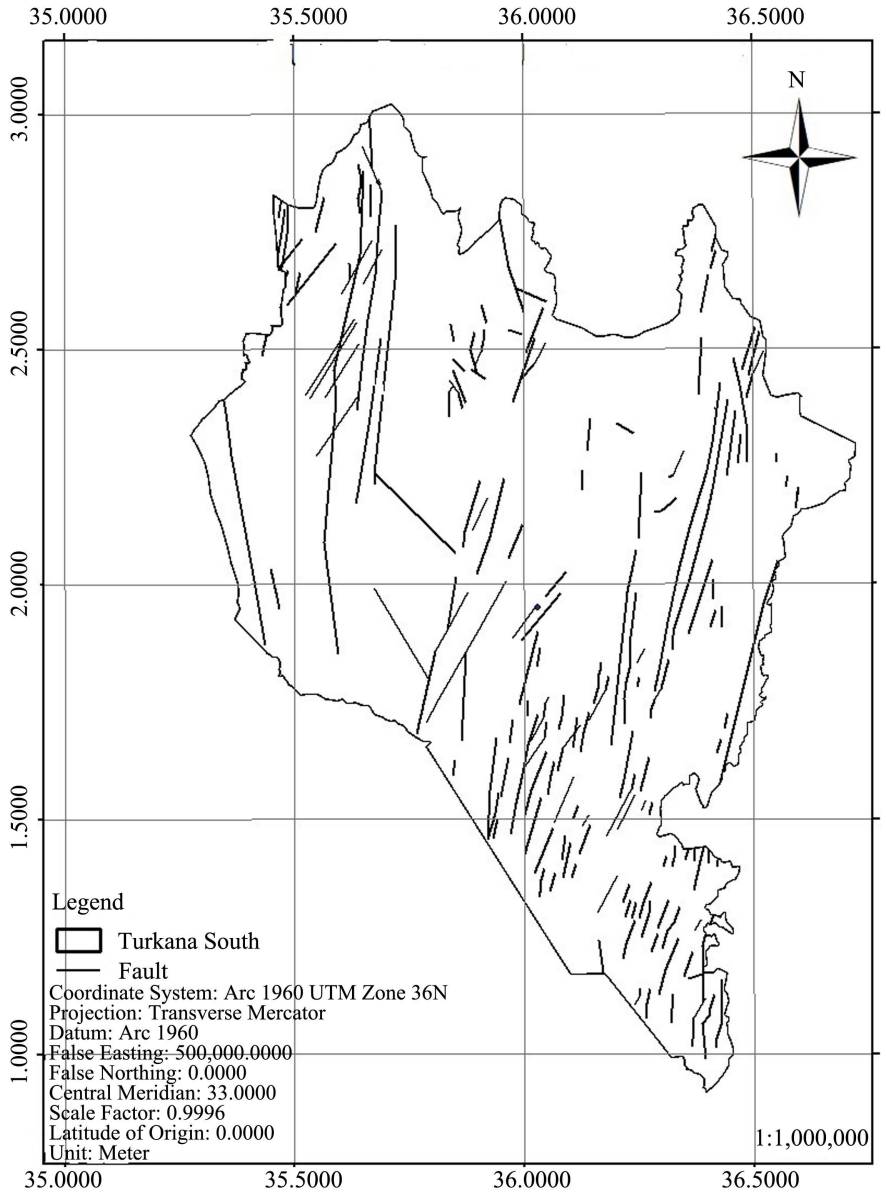

Figure 3. Structural geology map of Turkana South Subcounty.

In this equation $\bar{r}$ is a unit vector in the direction of increase in coordinate r, which is directed away from the center of reference at the mass M. The negative sign in the equation indicates that the force F acts in the opposite direction, toward the attracting mass M. The constant G, which converts the physical law to an equation, is the constant of universal gravitation. The second law of motion states that the rate of change of momentum of a mass is proportional to the force acting upon it and takes place in the direction of the force (Lowrie, 2007) which defines force (F) in terms of the acceleration (a) given to a mass (m) as Equation (3).

$$F = ma \tag{3}$$

According to Hinze et al. (2013), gravity applications include micro-scale sur-

veys in mapping physical property variations of the upper meter or two of the subsurface, or larger-scale applications for regional to global surveys designed to image the deeper variations of the Earth's crust, mantle, and core. The crust exhibits highly complex structural and compositional properties attributed to erosion, sedimentation, metamorphism, tectonics, and igneous activity, and the plastic movement of the mobile asthenosphere underlying the lithosphere occurred over time span of 4600-Myr. These processes have led to the differentiation of chemical elements, deposition of a variety of sediments, vertical and horizontal movements, zones of crustal weakness, and the focusing of geological processes, such as volcanism, which variations in the lithosphere control the formation and distribution of the Earth's resources, and volcanic, earthquake, and other natural hazards. The gravity survey investigates variation (gravity anomalies) in Earth's gravitational field generated by differences in density whose variations are induced by the presence of a causative body such as salt domes, granite plutons, sedimentary basins, heavy minerals like chromite and manganese, and faults and folds within the surrounding subsurface rocks (Haldar, 2018). The variations measured by gravity are dependent on Newton's universal law of gravitation, which takes into account the differential mass and the distance between the source and observation point (Hinze et al., 2013). The size of the anomalies primarily depends on the difference in density between host rocks and causative body, their geometrical form, and depth of occurrence (Haldar, 2018). The gravity anomalies are the differences between the observed and the theoretical field based on planetary considerations and the assumption of radial symmetry of the Earth layers (Hinze et al., 2013).

3.2. Gravity Data Collection

The gravity data used is secondary data collected in Kenya from 1955 to 1975 using La Coste & Romberg gravimeter G-16 with the reference point being Nairobi Pendulum Station (IGSN71 STATION "35716 A NAIROBI" VALUE. 9775260.7 g.u.). The calibration of the gravimeter was checked by measuring the gravity difference between Nairobi and Mombasa airport (STATION "35749 JII", VALUE 9780346.1 g.u.) and found correct to 1 in 5000.

The station elevations for the pre-1971 data were all measured using the "modified leapfrog" method (Searle, 1969) with two "Baromec" aneroid barometers supplemented later by two "Paulin" altimeters. The normal "leapfrog" is in principle the better method as index correction errors tend to cancel). Networks were constructed from interconnecting traverses and control points "tied into" whenever possible. Full terrain corrections were computed automatically for all stations for which adequate topographic maps, taking the earth's curvature into account and using a digital model of the East African topography based on the five-minute square (approx. 9 km.). Local terrain corrections (within 2 km. of the station) were included in the automatic computation by an interpolation method but where these were larger than 10 g.u. were always checked by zone chart. The accuracy of some of these methods has been studied by Stacey

and Stephens (1970) and an overall standard deviation of 10% of the total correction was expected.

3.3. Gravity Data Presentation

The gravity data used originates from the gravity measurements in Kenya done from 1955 to 1975. The data tables presented in this research contain three columns: 1) and 2) are the geographic co-ordinates in decimal degrees, and 3) is the observed absolute gravity.

The observed gravity data is presented as format of the Table 1 and the entire data in **Appendix** Table A1 and gravity units (g.u.) have been used throughout. (1 g.u. = 0.1 mgal = 10^{-6} m·s^{-2}). There is about 632 gravity readings measured and plotted in the area map (Figure 1) which have been reduced pursuant to the International Gravity Standardization Net 1971 and the National Gravity Reference Net of 1973.

3.4. Gravity Data Processing

The datum used in reducing the gravity observations is defined by the International Gravity Standardization Net adopted in 1971 (IGSN 71) (Morelli et al., 1971) together with the 1967 gravity formula (I.A.G. 1967) as recommended by the I.U.G.G. (Morelli, 1976). This required the subtraction of 137.5 g.u. from values that are referred to the Original Gravity Station (O.G.S.) primary net of Masson and Andrew (1962)—taking Nairobi "A" as the primary base. The tidal corrections to all the post 1971 data was done with the Base station readings made at intervals of up to 4 weeks, during the surveys, and indicated low long-term drift rates < 3 g.u. per month. The pre-1971 data were less accurate, perhaps ±4 g.u. It would have been possible to use the repeat readings during surveying to adjust the gravity values but as the average error in the elevations (±3 m) gives rise to an error of ±6 g.u. in the Bouguer anomalies this was not justified.

Table 1. Observed gravity data in the collected format.

Longitude (decimal Degrees)	Latitude (decimal Degrees)	Observed Gravity
35.5015	0.8562	9,774,101
35.5096	0.8932	9,774,078
35.5221	0.9600	9,773,840
35.5337	0.9391	9,773,949
35.5409	0.9763	9,774,107
35.5490	0.9835	9,774,245
35.5597	0.9998	9,774,603
35.0550	0.8690	9,774,699
35.0117	0.9115	9,774,921

The considered theoretical sea-level gravity, ϒ, at latitude Ø, was calculated from the 1967 gravity formula after the Geodetic Reference System 1967 (International Association of Geodesy, 1971) with the approximation (Equation (4)) whose accuracy is up to 0.04 g.u., being used.

$$\Upsilon = 9780318.5(1 + 0.005278895\sin^2\text{Ø} + 0.000023462\sin^4\text{Ø}) \text{ g.u.} \quad (4)$$

The correction −171.0 ± 0.5 g.u. can be applied to values of ϒ calculated with Cassinis (1930) formula within 5˚ of the equator.

The free air anomalies (F.A.A.) were calculated by use of the continuing upward of the sea level theoretical gravity ϒ to the measured station height by applying the free air correction factor which is then subtracted from the observed gravity g_o thus (Equation (5)):

$$\text{F.A.A.} = g_o - \left(\Upsilon - 3.086h\right) \text{g.u.} \left(h \text{ in m}\right) \quad (5)$$

The conventional constant factor was used throughout with the variation of the factor with latitude and elevation given as shown (Equation (6)) by Vyskocil (1960):

$$\text{F.A, Correction (g.u.)} = -(3.08772 + 0.00439\sin^2\text{Ø} - 0.72 \times 10^{-6}h)h \quad (6)$$

which implies an error at the equator, through using the constant quoted, of −1.0 g.u. at 1000 m. and +4.6 g.u. at 4000 m. These errors are unchanged upto 5˚ from the equator.

The "simple Bouguer anomalies" (S.B.A.) were determined by subtracting a calculated value from the F.A.A. (Equation (7)), which represents the effect of an slab considered to be infinite and horizontal of thickness equal to the station height h and density p (2.67×10^3 kg·m^{-3}).

$$\text{S.B.A.} = \text{F.A.A.} - 2\Pi Gph = \text{F.A.A.} - 1.119h \text{ g.u.} \quad (7)$$

The "complete Bouguer anomaly" (C.B.A.) should in principle be calculated by subtracting from the F.A.A. the effect at the observation point, of all masses outside the geoid. However, the attraction of topography beyond Hayford's Zone 0 is inconvenient to calculate (Bullard, 1936) and the "indirect effect" of the topography, causing the geoid to depart from the spheroid, becomes relatively large for such distant masses. Except where extreme elevation changes occur in relatively short distances, as occurs in New Guinea for example, (St. John & Green, 1967) the effect of the more distant topography will show slow spatial variation. For these reasons the convention of Heiskanen and Veninq (1958) was followed and an attempt was made to correct for those masses outside the geoid and within the outer limit of Hayford Zone 0 (166.7 km).

A terrain correction T was computed for stations, as the difference in gravity effect between the actual topography within 166.7 km. of the station and a disc of thickness equal to the station elevation, radius 166.7 km. and curved to the radius of the earth. A correction B was made to all stations for the gravity difference between the curved disc, just defined, and the infinite slab of the simple Bouguer correction (Bullard, 1936).

The value B (Equation (8)) was computed for elevations using different ap-

proximate methods including that of Takin and Talwani (1966) and finally the resultant in Equation (9) adopted.

$$B = 0.0134h - 3.5\times10^{-6}h^2 \text{ g.u.}\left(h \text{ in m}\right) \tag{8}$$

Thus

$$\text{C.B.A.} = \text{S.B.A.} + T - B \tag{9}$$

It should be noted that both T and B depend on the density. With this method of reduction, a constant density must be used and 2.67 × 10^3 kg·m^3 was used throughout. The Processed data presented in this research (**Table 2**) contain four columns: 1) and 2) are the geographic co-ordinates in decimal degrees, 3) is the observed absolute gravity, and 4) complete Bouguer anomalies. The data is presented in format as in the **Table 2** and the entire data in **Appendix Table A1**.

3.5. Gravity Data Analysis and Interpretation

Secondary gravity data was used where standard gravity corrections, including removal of the effect of instrument drift, tide, elevation and latitude were applied to the data. These corrections were carried out within the gravity processing package of Oasis Montaj. The corrected gravity values were contoured to produce anomaly maps. Gravity data analysis and interpretation was used to measure the differences in density on the earth's surface that indicate the underlying geologic structures.

The corrected gravity values were contoured to produce anomaly maps. Gravity data analysis and interpretation was used to measure the differences in density on the earth's surface that indicate the underlying geologic structures. The observed gravity data sets were reduced to complete bouguer anomaly data and they were gridded and contoured by using Geosoft Program Oasis Montaj to produce several maps. The corrected data (complete bouguer anomaly data) were plotted into bouguer anomaly maps which were filtered into regional (**Figure 6**) and residual (**Figure 7**) gravity anomaly maps. These maps show

Table 2. Processed gravity data as complete Bouguer anomaly.

Longitude in Degrees	Latitude in Degrees	Observed Gravity	Complete Bouguer Anomaly(CBA)
35.5015	0.8562	9,774,101	−1488
35.5096	0.8932	9,774,078	−1466
35.5221	0.9600	9,773,840	−1484
35.5337	0.9391	9,773,949	−1481
35.5409	0.9763	9,774,107	−1489
35.5490	0.9835	9,774,245	−1475
35.5597	0.9998	9,774,603	−1440
35.0550	0.8690	9,774,699	−1782
35.0117	0.9115	9,774,921	−1836

different high and low anomalous values through the survey area. The minimum curvature method was applied to determine the residual and the regional gravity anomalies. Algorithm was used where minimum-curvature gridding technique uses a two-dimensional (2-D) differential equation for the displacement of a thin sheet under the influence of point forces. The algorithm used after Webring (1981) was a keen in the minimization of aliasing in large gaps between adjacent data points. The minimum-curvature gridding algorithm was applied to the complete bouguer anomaly data to define the regional gravity field. The contours of the minimum-curvature regional gravity map were matched in the contouring as that of the complete bouguer anomaly and were as influenced by the features of interest.

The deployment of complex attributes (that is analytic signal and tilt derivative) of filtered Bouguer Gravity signal helped to extract properties of the source of the anomalous fields in the study area and thus the gridded analytic signal gravity maps (**Figure 8**). In processing of the complex attributes, a filter of passing the wavelengths of not more than 1 km was used on the complete bouguer anomaly gravity data resulting unto several maps (**Figures 6-8**) with the regional bouguer anomaly map (**Figure 4**) considered for determination of depths. The **Figure 5** shows a power spectrum curve of a line running in the E-W direction of the study area. The power spectrum curve is further divided into components as are related to gravity anomalies starting the deepest, to the shallow and later handling the noise sources.

The depth calculation by using Power Spectrum Curve Numbers (**Table 3**) were achieved by using the Equation (10) after Nadiah (2016), where the subsurface depth was calculated by the basis of difference of power spectrum. In the equation the depth value of positive ḍ indicates the mean depth along the gravity data profile.

$$|ḍ| = \frac{-1}{4\pi}\left(\frac{\log E_1 - \log E_2}{k_1 - k_2}\right) \tag{10}$$

Whereby the E_1 and E_2 stand for the power spectrum, k_1 and k_2 standing for the wave numbers. Equation (10) provides the depths, ḍ that are derived by getting the difference of the power spectrum curve slopes divided by -4π. Using the Equation (10) and reading the values of the Power Spectrum Curve Numbers from **Figure 5**, **Figure 9** and **Figure 10**, the values in **Table 3** were determined.

4. Results

Several outcomes of data analysis is presented under the gravity consideration in this study. The data presented include the regional bouguer anomaly maps (**Figure 6**), the residual bouguer gravity anomaly maps (**Figure 7**), and the analytic signal maps (**Figure 8**).

Equally power spectrum numbers were established and **Figure 9** displays the power spectrum curves as interpreted for a line along the E-W direction along latitude 2.261814 degrees, and the correlation of curvatures in the interpreted power spectrum and the depth estimate curves is given in **Figure 10**.

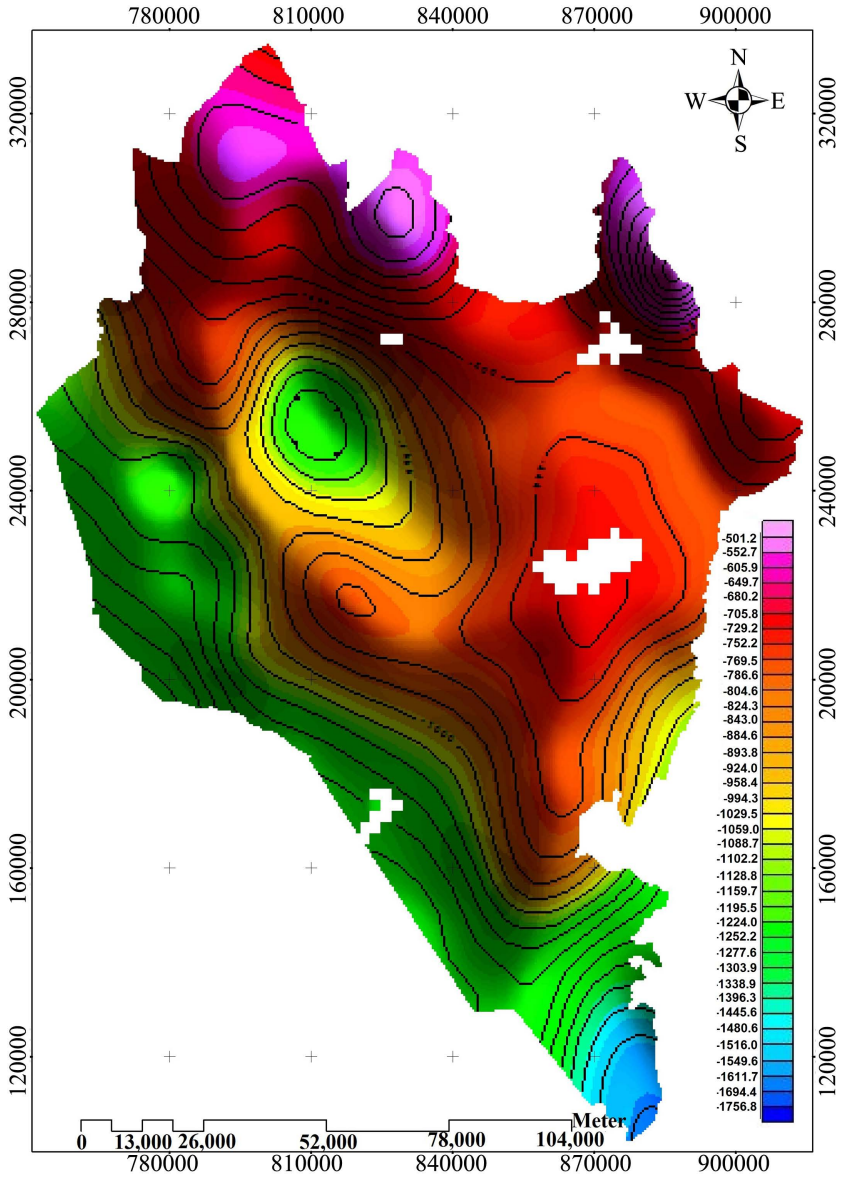

Figure 4. Regional bouguer anomaly map key in establishing of the power spectrum.

Table 3. Calculation for depths using power spectrum curve numbers.

Curve	|d|	4π	logE_1	logE_2	k_1	k_2	Depth
A	12.8	12.57142857	6	1	0.01	0.041	−12.83
B	4.6	12.57142857	1	−5.1	0.041	0.15	−4.452
C	1.1	12.57142857	−5.1	−6	0.15	0.217	−1.069

5. Discussion

The use of gravity data has demonstrated capability for monitoring lithological changes in large-scale in as a consequence differentiating basement and sedimentary of buried valleys. Gravity anomalies are associated with lateral contrasts in density and therefore deformation by faulting or folding will be manifested if

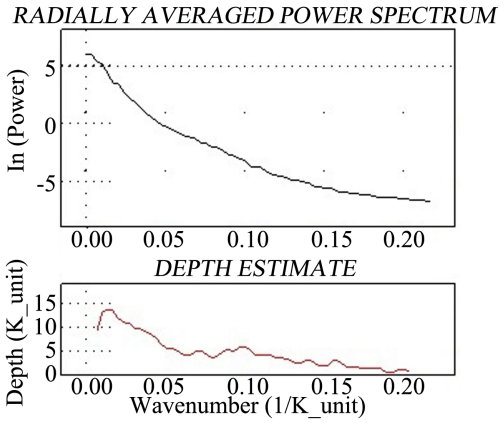

Figure 5. Complete bouguer anomaly spectrum.

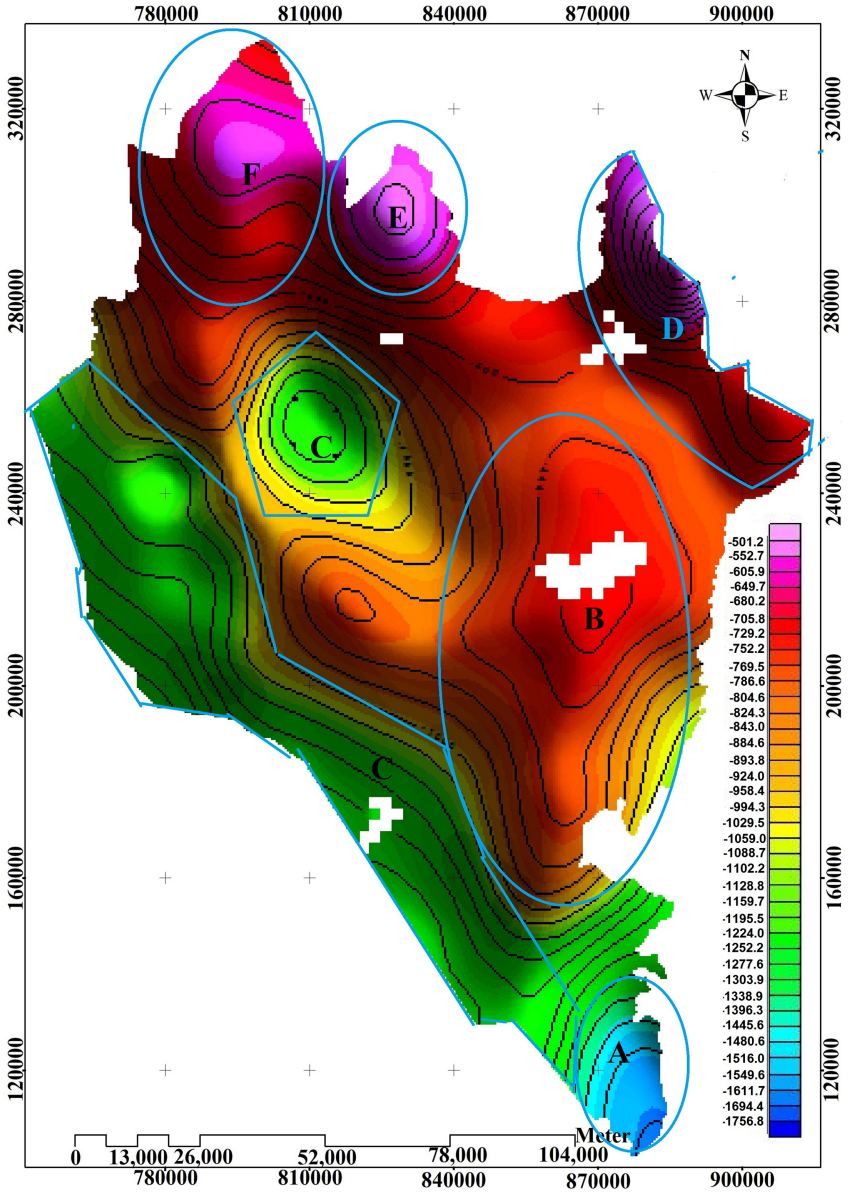

Figure 6. The regional bouguer anomaly map with contours.

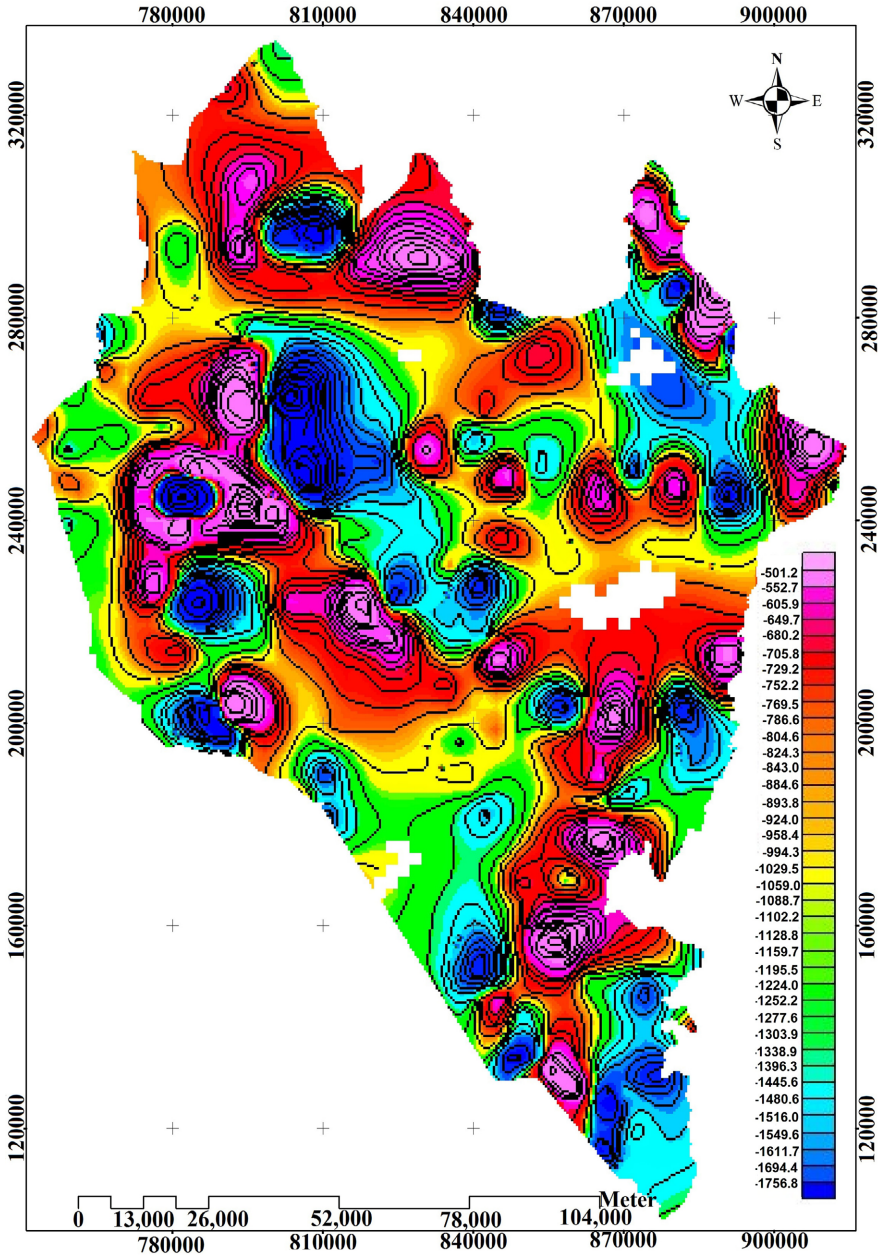

Figure 7. The residual bouguer gravity anomaly map with contours.

accompanied with lateral density changes, otherwise the vice versa is true. The area presents an overall range of Bouguer anomaly of −1756.8 g.u to −501.2 g.u, all negative, and the descriptions are enumerated in Table 4 in the different zones presented in the map (Figure 6). The regional anomaly gravity map presents high anomalies in the Northern region in the NW-SE trend and low anomalies in the southern trending in NW-SE, while the residual anomaly gravity map shows different trends for the low and high gravity anomalies.

The major rock groups in the study area have varying densities (Table 5) ranging from Sandstone beds with a density of 2050 kg/m^3 to Archean basement with densities in excess of 3200 kg/m^3.

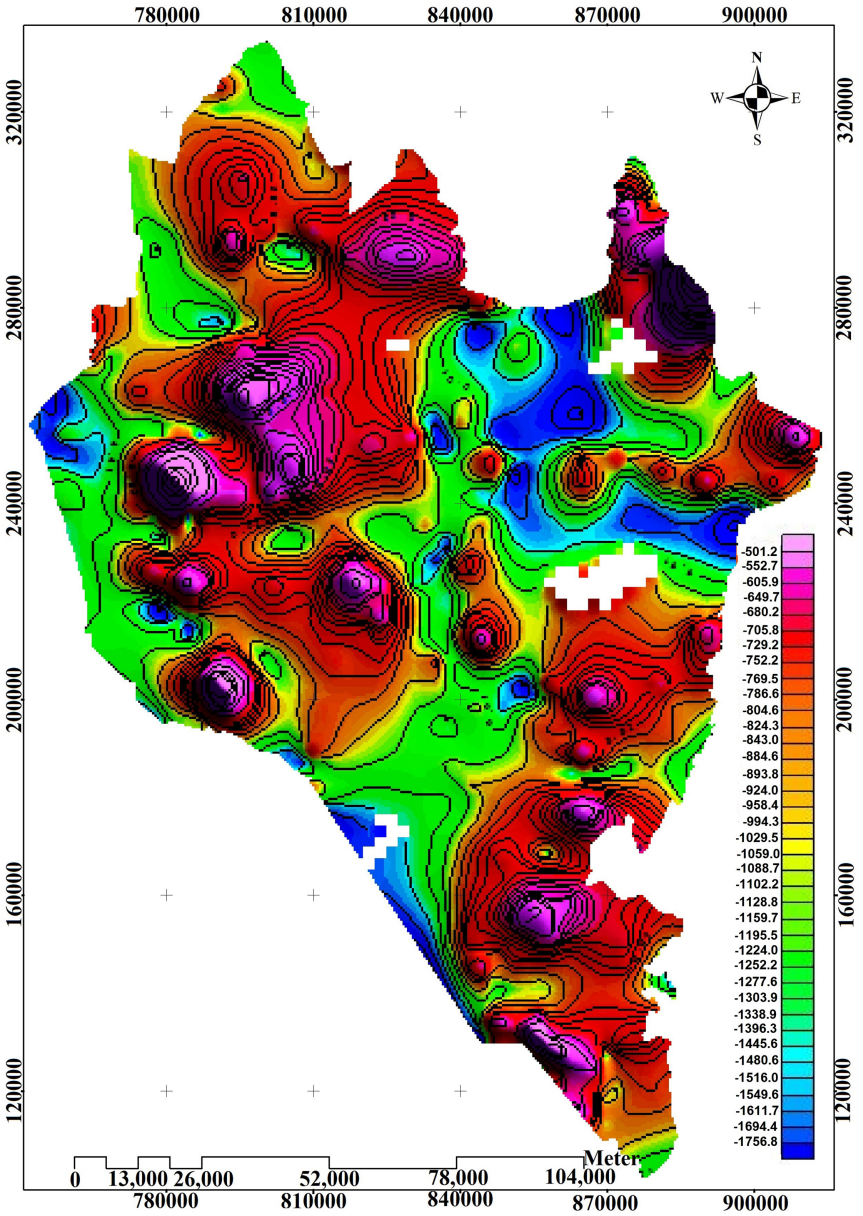

Figure 8. The analytic signal gravity map with contours.

Consequently, the gravity anomalies are well interpreted in line with the lithologies of the study area rather than the deformation of the same lithologies. Meaning the deformation in the area isn't accompanied with changes in densities of deformed lithologies. Therefore, analysis of Figure 6 (regional bouguer gravity anomaly map), and Figure 2 (lithology map) shows a good correlation. Zone A with pyroclastics overlying basement rocks with ~−1756.8 g.u to −1445.6 g.u. anomalous amplitude and Zone B with basalt, igneous rock, granite and acidic metamorphic rocks overlying basement with anomalous amplitude of ~−994.3 g.u. to −680.2 g.u. The pyroclastics, andesites, trachytes, phonolites, sandstone, greywacke and Eolian unconsolidated rock all overlying the basement dominate Zone C having low amplitude (~−1396.8 g.u to −1102.2 g.u). Zones D,

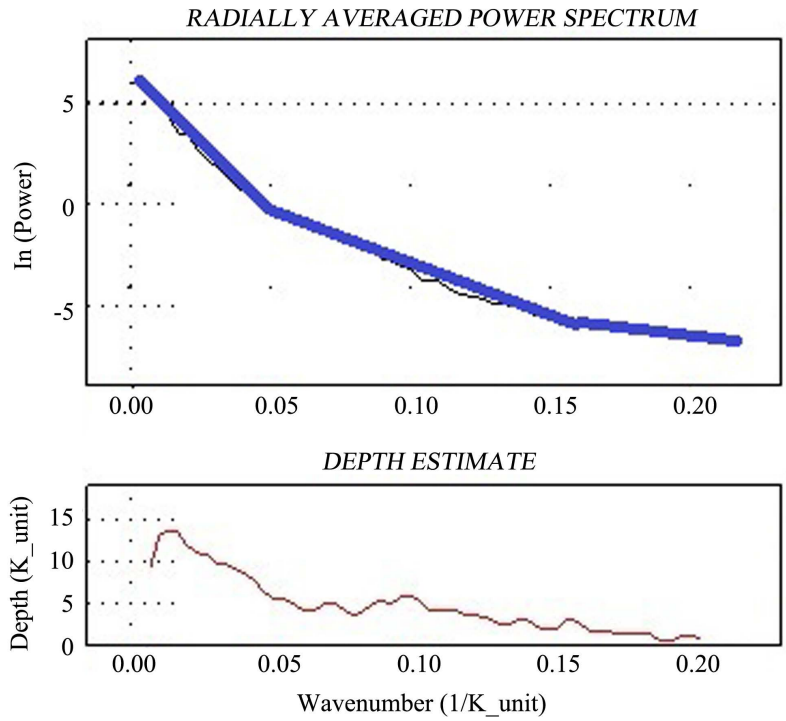

Figure 9. The interpreted power spectrum curves of a line along the E-W direction.

Table 4. Bouguer anomaly zone descriptions based on gravity pattern.

Zone	Characteristic Anomaly
A	Zone showing pattern at the SE lower corner of map showing lowest amplitude (~−1445.6 g.u. to −1756.8 g.u), further analysis in relation with geology and structural maps shows the contrast of high density pyroclastics overlying high density basement, probably tectonic events, faulting. The rocks here have low density variations compared to the basement rocks.
B	Zone of broad northerly trending bound feature in the eastern part of the area; indicating moderate amplitude (~−680.2 g.u. to −994.3 g.u). The area is covered by basalt, igneous rock, granite and acidic metamorphic rocks. These are rocks whose densities are closer to the basement density.
C	Zone C has the outstanding feature with north westerly continuous trend stretching from the SE to the west having low amplitude (~−1102.2 g.u to −1396.8 g.u). Correlation with geological map indicates that the surface is covered with pyroclastics, andesites, trachytes, phonolites, sandstone, greywacke and Eolian unconsolidated rock all overlying the basement. The rocks here have recognizable density variations from the one by basement rocks.
D, E, F	Zone of northerly trending parallel features covering the northern part; showing alternating moderate to high amplitude (~−501.2 g.u to −994.3 g.u). The geology of the sections is mainly of granite and acidic metamorphic rocks, andesites, basalts, and pyroclastics.

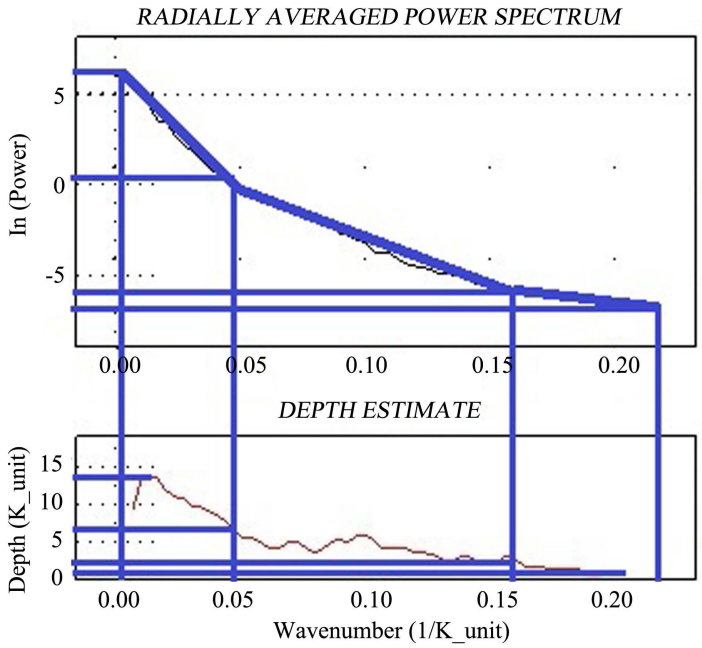

Figure 10. The correlation of curvatures in the interpreted power spectrum and the depth estimate curves.

Table 5. Densities of Common Rocks in the study area.

Rocks	Density (10^3 kg/m^3)
Amphibolites	2.79 - 3.14
Basalt	2.70 - 3.20
Gabbro	2.85 - 3.12
Gneiss	2.61 - 2.99
Granite	2.52 - 2.75
Quartzite	2.60 - 2.70
Rhyolite	2.40 - 2.60
Sandstone	2.05 - 2.55
Schist	2.50 - 2.90

E, F portents alternating moderate to high amplitude (~−994.3 g.u to −501.2 g.u) representing geology of granite and acidic metamorphic rocks, andesites, basalts, and pyroclastics overlying the basement.

The residual anomaly gravity map indicates that the area is affected with faulting with faults running in the NE-SW and N-S trends. This is seen in residual anomaly gravity contour map in that the edges of contoured map (Figure 7) matches well with points of high faulting in the structural geology map (Figure 3). The technique of analytical signal calls for its interpretation in conjunction with other geological and geophysical information to maximize on its

results. Thus the calibration of the analytic signal map (Figure 8) is done where points of high anomaly values matches well with areas which in geological map (Figure 2) are covered by igneous intrusive rocks considered to be of high density or fluvial deposits considered to be deposits of heavy minerals. This is evident also in the analytical signal map for these formations poses high density in comparison to surrounding rocks.

The Figure 9 displays the power spectrum curves as interpreted for a line along the E-W direction along latitude 2.261814 degrees. Accordingly, the depths related to the gravity sources have been calculated using the curve slope obtained from Figure 10. The Figure 10 shows comparison between the graphs of radially averaged power spectrum and the depth estimate graph.

Fundamentally, the power spectrum curves are separated into three components interrelated with gravity anomalies originating from the deepest formations, the shallow formations and structures and finally from the noise sources. By application of Equation (10), the depths to gravity anomaly sources have been calculated using the three slope curves. The radially averaged power spectrum curve is presented as In(Power) in the Y-axis and the Wave Number (1/K_Unit) in the X-axis. Equally the depth estimate has been given as Depth (K_Unit) in the Y-axis and the Number (1/K_Unit) in the X-axis. The Table 6 presents estimated and calculated depths t subsurface sources of gravity anomalies.

Based on the research, the different anomalies relate well with different rock densities in the study area along the line profile. The gravity highs are noted in the eastern point and are associated with andesites, trachytes, basalts and igneous rocks, while the gravity lows are associated with sandstone, greywacke, arkose, and eolian unconsolidated rock. By the use of the Power spectrum analysis the showing of the depth of the deepest basement rock is 12.8 km which is in the eastern flank, while the shallowest to the basement of 1.1 km to the western flank.

The bouguer anomaly maps happen to always acts as the best and indeed display the best subsurface density changes of the bedrock in the areas of interest. The variations of the bouguer anomaly have been enhanced by calculating 2nd derivative and horizontal gradient (tilt derivative) relief maps. These maps have helped in recognizing, discovering, and categorizing formations and structures affecting gravity. Local variation of gravity is well observed in the residual bouguer anomaly, tilt derivative and analytic signal maps where, the sources are aligned to quantities relating to position, shape and structure of geological formations.

Table 6. Depth estimation for unconformity bedrock.

Curve	Assumed Depth (km)	Calculated Depth (km)
A	13	12.8
B	5	4.1
C	1.4	1.1

6. Conclusion

The gravity method used in this study has been instrumental and the conclusion of results of interpretation is that the area is affected by different fault elements trending NE-SW, N-S and minor in the E-W reflecting the orientation of different lithologies, which can be tied to past tectonic activities. The gravity anomalies are well interpreted in line with the lithologies of the study area rather than the deformation of the same lithologies. There is observed high values of gravity anomaly values (ranging from −880.2 to −501.2 g.u.) where there are eolian unconsolidated rocks overlying the basement as compared to low gravity anomaly values (ranging from −1338.9 to −1088.7 g.u.) where the andesites, trachytes and phonolites overly the basement. The different regional gravity anomalies relate well with different rock densities in the study area along the line profile for radially averaged power spectrum. The gravity highs are noted in the eastern point and are associated with andesites, trachytes, basalts and igneous rocks, while the gravity lows are associated with sandstone, greywacke, arkose, and eolian unconsolidated rock. The utilization of the information from the power spectrum analysis demonstrates that the depth to the deepest basement rock is 12.8 km which is in the eastern flank, while the shallowest to the basement of 1.1 km to the western flank.

Acknowledgements

Special appreciations go to the Ministry of Petroleum and Mining, Kenya from whom geological and topographic maps were obtained, which were useful in the production of the final geological map of the area. To the survey of Kenya which was instrumental in provision of data used, I am indebted. I also wish to recognize the prayers, efforts, encouragement, humour and cooperation received from my wife Lydia Gesare and our Children (Amygrace Kerubo Tsitsi, Merrybell Meita, and Madiba Mandela) during the entire period of this research. They allowed me to use the meagre family resources for the research and am dearly indebted.

Conflicts of Interest

The author declares no conflicts of interest regarding the publication of this paper.

References

Balsubramanian, A. (2007). *Methods of Groundwater Exploration*.

Bullard, E. C. (1936). Gravity Measurements in East Africa. *Proceedings of the Royal Society of London. Series A, 235,* 445-531. https://doi.org/10.1098/rsta.1936.0008

Cassinis, G. (1930). Sur l'adoption d'une formule internationale pour la pesanteur normale. *Bulletin Géodésique, 26,* 40-49. https://doi.org/10.1007/BF03030025

Chandler Val, W. (1994). *Gravity Investigation for Potential Ground-Water Resources in Rock County, Minnesota*. Report of Investigations 44, University of Minnesota.

Feibel, C. S. (2011). A Geological History of the Turkana Basin. *Evolutionary Anthropology, 20,* 206-216. https://doi.org/10.1002/evan.20331

Hakim, S. (2018). *Microgravity and Its Applications in Geosciences*.

Haldar, S. K. (2018). *Mineral Exploration: Principles and Applications* (2nd ed.). Joe Hayton. https://doi.org/10.1016/B978-0-12-814022-2.00001-0

Handayani, L., Wardhana, D. D., Hartanto, P., Delinom, R., Sudaryanto, Bakti, H., & Lubis, R. F. (2018). Gravity Survey of Groundwater Characterization at Labuan Basin. *IOP Conference Series: Earth and Environmental Science, 118,* Article ID: 012015. https://doi.org/10.1088/1755-1315/118/1/012015

Heiskanen, W. A., & Venning, M. F. A. (1958). *The Earth and Its Gravity Field*. McGraw-Hill.

Hinze, W. J., Ralph, R. B., von Frese, & Saad, A. H. (2013). *Gravity and Magnetic Exploration: Principles, Practices, and Applications*. Cambridge University Press.

Idris, M. G., Abba, S. I., Said, B. U., & Abdullahi, M. B. (2015). The Underground Water Investigations Using Self-Potential Geophysical Survey A Case Study of Buk Old Campus by the Application of Computer Modeling Sofware (Matlab) Kano, Nigeria. *International Journal of Advanced Technology in Engineering and Science, 3,* 680.

International Association of Geodesy (1971). *Geodetic Reference System 1967*. Special Publication No. 3, Bureau Central de l'Association Internationale de Geodesie.

Lowrie, W. (2007). *Fundamentals of Geophysics* (2nd Ed.). Swiss Federal Institute of Technology. https://doi.org/10.1017/CBO9780511807107

Masson, S. D. J., & Andrew, E. M. (1962). Gravity Meter Primary Station Net in East and Central Africa. *The Geophysical Journal of the Royal Astronomical Society, 7,* 65-85. https://doi.org/10.1111/j.1365-246X.1962.tb02253.x

Morelli, C. (1976). Modern Standards for Gravity Surveys. *Geophysical Prospecting, 24,* 198-199. https://doi.org/10.1111/j.1365-2478.1976.tb00391.x

Morelli, C., Gantar, C., Honkasalo, T., McConnell, R. K., Tanner, I. G., Szabo, B., & Whalen, C. T. (1971). *The International Gravity Standardization Net 1971*.

Roche, H., Brugal, J.-P., Delagnes, A., Feibel, C., Harmand, S., Kibunjia, M., Prat, S., & Texier, P.-J. (2004). Plio-Pleistocene Archaeological Sites in the Nachakui Formation, West Turkana, Kenya: Synthetic Results 1997-2001. *Comptes Rendus Palevol, 2,* 663-673. https://doi.org/10.1016/j.crpv.2003.06.001

Rooney, T. O., Wallace, P. J., Muirhead, J. D. Chiasera, B. R., Steiner, A., Girard, G., & Karson, J. A. (2022). Transition to Magma-Driven Rifting in the South Turkana Basin, Kenya. *Journal of the Geological Society, 179,* jgs2021-160. https://doi.org/10.1144/jgs2021-160

Schlüter, T. (1997). *Geology of East Africa*. Gebröder Borntraeger.

Searle, R. C. (1969). *Barometric Hypsometry and a Geophysical Study of Part of the Gregory Rift Valley in Kenya*. Thesis, University of Newcastle upon Tyne.

St. John, V. P., & Green, R. (1967). Topographic and Isostatic Corrections to Gravity Surveys in Mountainous Areas. *Geophysical Prospecting, 15,* 151-162. https://doi.org/10.1111/j.1365-2478.1967.tb01778.x

Stacey, R. A., & Stephens, L. E. (1970). *Procedures for Calculating Terrain Corrections for Gravity Measurements*. Publications of the Dominion Observatory, Ottawa, Vol. 39, No. 10, Canada Department of Energy, Mines and Resources. https://doi.org/10.4095/313017

Sultan, A. S. A., Hassan, S. S., Ahmed, M., & Al Dabour (2015). *Integrated Geophysical*

Interpretation on the Groundwater Aquifer (At the North).

Takin, M., & Talwani, M. (1966). Rapid Computation of the Gravitational Attraction of Topography on a Spherical Earth. *Geophysical Prospecting, 14,* 119-142. https://doi.org/10.1111/j.1365-2478.1966.tb01750.x

Truckle, P. H. (1977). *The Geology of the Are7& to the South of Lokori, South Turkana, Kenya*. Thesis, University of Leicester.

Vyskocil, V. (1960). Anomaly Field of Gravity in Gravimetric Prospecting. Travaux Inst. Geophys. Acad. Tchécosl. Sci. No 131.

Webring, M. (1981). *MINC: A Gridding Program Based on Minimum Curvature*. U.S. Geol. Surv., Open-File Rep. 81-1224. https://doi.org/10.3133/ofr811224

Appendix

Table A1. Gravity observed and processed gravity data as complete Bouguer anomaly.

Longitude Degrees	Latitude Degrees	Observed Gravity	Complete Bouguer Anomaly
35.5015	0.8562	9,774,101	−1488
35.5096	0.8932	9,774,078	−1466
35.5221	0.9600	9,773,840	−1484
35.5337	0.9391	9,773,949	−1481
35.5409	0.9763	9,774,107	−1489
35.5490	0.9835	9,774,245	−1475
35.5597	0.9998	9,774,603	−1440
35.0550	0.8690	9,774,699	−1782
35.0117	0.9115	9,774,921	−1836
35.0596	0.9576	9,774,859	−1799
35.0856	0.9241	9,774,873	−1787
35.1186	0.8825	9,775,029	−1761
35.1251	0.8508	9,774,922	−1745
35.1763	0.8716	9,774,759	−1726
35.2257	0.8743	9,774,754	−1708
35.2533	0.8545	9,774,679	−1698
35.3000	0.8301	9,774,673	−1657
35.6073	0.3695	9,776,515	−1561
35.6145	0.8984	9,776,598	−1556
35.6154	0.9165	9,776,664	−1545
35.0226	0.9355	9,776,656	−1002
35.6217	0.9545	9,776,591	−1573
35.6128	0.9870	9,776,560	−1492
35.0093	0.9693	9,774,764	−1632
35.0434	0.9836	9,774,764	−1815
35.6944	0.8677	9,776,058	−2168
35.6908	0.902	9,776,125	−2089
35.6899	0.9291	9,776,163	−2038
35.6837	0.9779	9,776,137	−1995
35.7187	0.9282	9,776,065	−1920
35.7429	0.9191	9,775,845	−1816

Continued

35.7626	0.9029	9,775,881	−1742
35.7923	0.8866	9,775,836	−1625
35.8129	0.8649	9,775,445	−1709
35.8093	0.8396	9,775,388	−1760
35.8264	0.8802	9,775,787	−1675
35.8407	0.8793	9,775,586	−1703
35.8497	0.8647	9,775,909	−1666
35.8757	0.8955	9,770,372	−1687
35.9018	0.8829	9,776,536	−1680
35.9071	0.8621	9,776,599	−1648
35.9098	0.8377	9,776,042	−1610
35.9934	0.9352	9,777,238	−1403
35.9664	0.9515	9,777,087	−1491
35.9001	0.9316	9,776,980	−1547
35.9458	0.9108	9,776,864	−1584
35.9314	0.8865	9,776,636	−1612
36.1790	0.8811	9,776,751	−1292
36.7447	0.8951	9,775,392	−1401
36.7590	0.9349	9,775,481	−1344
36.7536	0.9764	9,775,472	−1218
36.7851	0.9023	9,775,522	−1347
36.5991	0.9754	9,774,873	−1492
36.5974	0.9203	9,774,894	−1516
36.1072	0.8991	9,777,286	−1293
36.1180	0.9217	9,777,241	−1288
36.1323	0.9534	9,777,368	−1197
36.1466	0.9796	9,777,462	−1165
36.1682	0.9877	977,724	−1162
36.2849	0.9761	9,776,392	−1454
36.2732	0.9327	9,776,412	−1455
36.2751	0.8902	9,776,486	−1453
36.0300	0.9424	9,777,341	−1314
36.0470	0.9578	9,777,379	−1262
36.0595	0.9949	9,777,487	−1211

Continued

36.0327	0.8918	9,777,211	−1388
36.0354	0.9144	9,777,263	−1364
36.0551	0.9208	9,777,285	−1334
36.0758	0.9027	9,777,276	−1312
36.0991	0.8973	9,777,291	−1297
36.1252	0.8973	9,777,221	−1302
36.1422	0.8919	9,777,193	−1264
36.0048	0.9641	9,777,336	−1341
36.0147	0.9975	9,777,408	−1309
36.3001	1.0050	9,776,788	−1468
35.5705	1.0052	9,774,434	−1455
35.6128	1.0078	9,776,543	−1463
36.6126	1.0107	9,775,014	−1427
36.1888	1.0122	9,777,513	−1142
36.7266	1.0225	9,775,368	−1293
36.6494	1.0234	9,775,282	−1327
36.0236	1.0265	9,777,424	−1322
36.1520	1.0266	9,777,614	−1109
36.2085	1.0275	9,777,460	−1184
36.1798	1.0284	9,777,561	−1120
35.9566	1.0292	9,777,035	−1479
36.0452	1.0292	9,777,479	−1284
36.3199	1.0294	9,776,873	−1495
36.2400	1.0303	9,777,315	−1277
35.5758	1.0305	9,774,089	−1461
35.6191	1.034	9,776,669	−1450
36.0703	1.0356	9,777,571	−1210
36.2660	1.0393	9,777,103	−1407
36.2893	1.0421	9,776,934	−1484
35.9225	1.0473	9,776,891	−1533
35.6290	1.0503	9,776,734	−1455
36.0398	1.0509	9,777,426	−1327
36.3297	1.0548	9,776,895	−1495
36.6808	1.0560	9,775,263	−1296

Continued

36.7086	1.0578	9,775,390	−1261
35.5830	1.0667	9,774,774	−1432
35.8956	1.0672	9,776,733	−1533
35.5946	1.0676	9,774,699	−1416
35.6063	1.0676	9,774,948	−1396
36.0792	1.0717	9,777,577	−1221
35.6335	1.0729	9,776,704	−1452
36.0487	1.0753	9,777,483	−1290
35.6117	1.0803	9,775,356	−1405
36.5838	1.0830	9,774,720	−1364
36.3387	1.0837	9,776,935	−1494
36.6664	1.0912	9,774,932	−1290
35.8822	1.0925	9,776,791	−1390
35.6186	1.0938	9,775,779	−1407
36.6925	1.0966	9,775,226	−1280
35.6344	1.0973	9,776,622	−1423
36.0648	1.0988	9,777,480	−1316
35.6224	1.1019	9,776,076	−1413
35.8777	1.1088	9,776,667	−1279
36.0792	1.1106	9,777,560	−1269
35.6251	1.1110	9,776,194	−1409
35.8643	1.1115	9,776,483	−1264
36.3261	1.1180	9,777,003	−1469
35.6421	1.1218	9,776,705	−1430
36.2291	1.1243	9,776,813	−1231
36.0810	1.1268	9,777,578	−1262
35.8499	1.1287	9,776,832	−1259
36.2138	1.1288	9,776,725	−1206
36.2452	1.1297	9,776,875	−1239
36.2874	1.1297	9,776,869	−1451
36.2749	1.1306	9,776,878	−1383
36.2605	1.1324	9,776,858	−1297
36.3099	1.1325	9,776,911	−1489
36.2048	1.1351	9,776,623	−1201

Continued

35.3588	1.1364	9,772,924	−1633
36.3251	1.1370	9,777,043	−1442
36.5011	1.1399	9,774,944	−1490
36.6340	1.1418	9,774,592	−1321
36.1976	1.1477	9,776,606	−1192
36.2551	1.1487	9,776,733	−1263
36.2369	1.1532	9,777,191	−1138
36.4580	1.1534	9,775,945	−1471
36.2901	1.1550	9,776,915	−1420
36.1815	1.1567	9,776,577	−1181
36.2291	1.1577	9,777,260	−1110
36.2569	1.1577	9,776,742	−1259
36.0971	1.1593	9,777,662	−1270
36.1463	1.1594	3,777,231	−1195
35.6488	1.1596	9,776,776	−1426
35.6492	1.1598	9,776,773	−1430
35.8293	1.1604	9,776,946	−1309
36.2228	1.1649	9,777,285	−1101
36.3512	1.1687	9,777,022	−1480
36.1105	1.1693	9,777,543	−1285
36.1303	1.1693	9,777,437	−1232
35.6497	1.1696	9,776,752	−1431
36.3530	1.1696	9,777,021	−1480
36.1734	1.1712	9,775,994	−1253
35.3274	1.1717	9,773,048	−1675
36.2102	1.1730	9,777,231	−1087
35.8149	1.1757	9,777,021	−1279
36.1842	1.1757	9,776,581	−1163
36.1617	1.1784	9,776,803	−1180
36.4140	1.1823	9,776,109	−1487
36.1043	1.1829	9,777,644	−1290
35.8006	1.1848	9,777,040	−1300
36.2461	1.1866	9,776,792	−1221
36.6196	1.1870	9,774,253	−1294

Continued

35.6516	1.1904	9,776,708	−1434
36.2317	1.1911	9,776,742	−1197
36.1949	1.1929	9,776,663	−1172
36.2093	1.1929	9,776,778	−1161
36.2183	1.1929	9,776,758	−1176
36.1968	1.1939	9,777,876	−871
36.1823	1.1983	9,776,627	−1211
35.7270	1.2020	9,776,937	−1516
36.1213	1.2046	9,777,647	−1327
36.1653	1.2046	9,777,125	−1236
35.6561	1.2048	9,776,788	−1437
35.2825	1.2052	9,773,379	−1711
35.6776	1.2093	9,776,849	−1546
36.1024	1.2100	9,777,671	−1264
36.1410	1.2100	9,777,492	−1305
35.7611	1.2146	9,776,976	−1404
35.6965	1.2156	9,776,872	−1613
35.6552	1.2283	9,776,949	−1423
36.1060	1.2360	9,777,706	−1229
36.5025	1.2475	9,774,167	−1245
35.6453	1.2482	9,776,784	−1430
35.2484	1.2522	9,773,603	−1737
35.1694	1.2568	9,774,027	−1752
35.6301	1.2600	9,776,630	−1435
35.1918	1.2604	9,773,754	−1744
35.2313	1.2694	9,773,700	−1731
35.1613	1.2767	9,774,594	−1774
35.6283	1.2781	9,776,724	−1437
35.1712	1.2785	9,774,949	−1781
36.6160	1.2792	9,774,572	−1300
35.1586	1.2866	9,774,313	−1744
35.6202	1.2925	9,776,675	−1447
35.1892	1.3002	9,775,149	−1762
36.1454	1.3004	9,777,835	−1190

Continued

36.0996	1.3031	9,777,789	−1140
36.6195	1.3099	9,774,956	−1324
35.2053	1.3101	9,775,228	−1744
36.8611	1.3102	9,776,746	−1255
35.2269	1.3155	9,775,173	−1754
36.3663	1.3196	9,777,672	−1300
36.0843	1.3301	9,777,500	−1221
35.2530	1.3339	9,775,531	−1712
35.6266	1.3350	9,776,859	−1469
36.8611	1.3373	9,776,856	−1227
36.1561	1.3429	9,777,944	−1086
35.2018	1.3445	9,775,384	−1744
36.6303	1.3515	9,775,233	−1296
36.3644	1.3522	9,777,798	−1235
36.2522	1.3547	9,778,030	−1071
36.2711	1.3557	9,778,021	−1084
36.2378	1.3601	9,778,062	−1034
36.0796	1.3609	9,777,626	−1245
35.6311	1.3648	9,776,895	−1511
36.1759	1.3655	9,778,029	−1028
36.2926	1.3656	9,778,016	−1085
35.2458	1.3670	9,775,309	−1659
36.3590	1.3711	9,777,853	−1173
36.2208	1.3719	9,778,130	−965
36.3779	1.3748	9,777,802	−1187
36.3159	1.3756	9,777,987	−1097
35.6077	1.3757	9,776,850	−1437
36.3411	1.3783	9,777,932	−1123
35.1892	1.3815	9,775,406	−1706
36.6284	1.3823	9,775,381	−1302
35.2593	1.3869	9,775,455	−1636
36.0645	1.3880	9,777,481	−1249
36.1857	1.3890	9,778,143	−930
36.3752	1.3901	9,777,798	−1154

Continued

36.1992	1.3908	9,778,159	−929
36.1354	1.3926	9,777,883	−1068
35.5943	1.3947	9,776,877	−1451
35.3330	1.3995	9,775,831	−1628
36.0385	1.4015	9,777,415	−1249
35.5656	1.4038	9,776,886	−1454
35.3455	1.4067	9,775,646	−1612
35.2818	1.4086	9,775,548	−1632
35.3195	1.4103	9,775,735	−1619
36.6661	1.4112	9,775,673	−1792
35.2997	1.4113	9,775,636	−1620
36.2027	1.4116	9,778,236	−861
36.8539	1.4132	9,776,732	−1215
36.0187	1.4141	9,777,243	−1251
35.5395	1.4146	9,776,824	−1458
35.200	1.4159	9,775,567	−1681
35.3456	1.4230	9,775,873	−1588
36.2638	1.4289	9,778,221	−889
35.5252	1.4327	9,776,797	−1476
36.1399	1.4359	9,777,871	−1011
36.2090	1.4378	9,778,260	−863
35.3537	1.4383	9,775,945	−1584
35.2189	1.4394	9,775,696	−1659
36.0043	1.4394	9,777,045	−1242
36.8466	1.4449	9,776,926	−1154
36.7047	1.4529	9,775,779	−1271
35.5055	1.4599	9,776,866	−1515
35.3698	1.4618	9,776,123	−1549
35.2288	1.4647	9,775,769	−1687
36.2117	1.4659	9,778,298	−865
35.3726	1.4691	9,776,115	−1548
35.4875	1.4780	9,776,963	−1534
35.3762	1.4790	9,776,171	−1555
36.1443	1.4820	9,777,899	−979

Continued

35.2486	1.4846	9,775,687	−1726
35.3851	1.4862	9,776,234	−1530
35.5315	1.4870	9,777,010	−1511
36.8367	1.4883	9,776,887	−1122
36.2170	1.4894	9,778,339	−868
35.3932	1.4952	9,776,386	−1520
35.4669	1.4961	9,776,808	−1557
35.4049	1.4970	9,776,424	−1504
36.7765	1.4981	9,776,027	−1202
36.7253	1.4990	9,776,004	−1217
35.6743	1.5021	9,777,073	−1305
35.4049	1.5043	9,776,525	−1501
36.3472	1.5049	9,777,133	−896
35.2639	1.5053	9,775,715	−1712
36.6624	1.5071	9,776,105	−1233
36.4406	1.5095	9,777,044	−1195
36.6049	1.5142	9,775,823	−1205
36.2188	1.5156	9,778,355	−884
35.4094	1.5160	9,776,599	−1488
36.5259	1.5187	9,777,731	−1200
36.8385	1.5271	9,776,883	−1112
35.4103	1.5287	9,776,681	−1471
36.1371	1.5290	9,778,033	−956
35.7049	1.5292	9,777,128	−1268
35.4355	1.5296	9,776,788	−1504
35.2702	1.5297	9,775,036	−1661
35.4211	1.5305	9,776,682	−1481
35.4472	1.5322	9,776,940	−1509
35.5646	1.5339	9,777,125	−1442
36.2313	1.5373	9,778,416	−859
36.7343	1.5451	9,776,113	−1187
35.7166	1.5527	9,777,156	−1243
36.8286	1.5561	9,776,841	−1090
36.2520	1.5581	9,778,503	−819

Continued

35.5846	1.5628	9,777,154	−1361
35.4490	1.5675	9,776,873	−1517
35.7337	1.5735	9,777,255	−1212
36.1235	1.5787	9,778,082	−988
36.2654	1.5789	9,778,695	−781
36.7252	1.5948	9,776,276	−1171
35.7490	1.5979	9,777,310	−1180
35.5820	1.6044	9,777,208	−1340
36.0876	1.6067	9,778,082	−1042
36.2779	1.6069	9,778,886	−751
35.4553	1.6091	9,776,806	−1586
36.8231	1.6112	9,776,722	−1090
35.7706	1.6249	9,777,428	−1242
36.7467	1.6292	9,776,494	−1074
36.2779	1.6322	9,778,843	−809
36.7755	1.6428	9,776,676	−1054
35.6090	1.6441	9,777,197	−1277
35.4617	1.6452	9,776,978	−1494
35.7751	1.6475	9,777,506	−1223
36.0713	1.6491	9,778,138	−1045
36.8087	1.6609	9,776,629	−1050
35.7635	1.6728	9,777,491	−1177
36.3084	1.6729	9,778,782	−878
36.2668	1.6765	9,778,781	−840
35.4734	1.6769	9,777,055	−1528
36.3506	1.6811	9,778,777	−924
35.6297	1.6812	9,777,185	−1240
35.7419	1.6819	9,777,391	−1173
36.3748	1.6821	9,778,749	−942
36.4170	1.6821	9,778,646	−1012
36.0460	1.6852	9,778,151	−1012
36.4440	1.6903	9,778,618	−1038
35.7123	1.6991	9,777,282	−1180
36.7916	1.7007	9,776,711	−1034

Continued

35.4806	1.7040	9,777,065	−1450
36.2713	1.7045	9,778,700	−771
35.7743	1.7099	9,777,491	−1185
35.6818	1.7200	9,777,171	−1174
35.6270	1.7209	9,777,253	−1237
36.2517	1.7262	9,778,367	−804
36.0425	1.7331	9,778,163	−970
36.4448	1.7391	9,778,687	−1033
35.6486	1.7417	9,777,211	−1200
35.4807	1.7428	9,777,222	−1395
35.6199	1.7463	9,777,288	−1248
35.7860	1.7505	9,777,437	−1108
35.4888	1.7582	9,777,215	−1381
36.7888	1.7591	9,776,746	−1101
36.2499	1.7596	9,778,269	−785
36.0245	1.7737	9,778,204	−952
36.4717	1.7834	9,778,739	−1025
35.7987	1.7885	9,777,678	−1032
36.0855	1.7901	9,778,343	−893
36.1385	1.7902	9,778,380	−880
35.6173	1.7933	9,777,297	−1258
36.7969	1.7938	9,776,818	−1086
36.2507	1.7976	9,778,259	−773
36.3064	1.8103	9,778,805	−702
36.4806	1.8223	9,778,806	−977
35.6140	1.8264	9,777,719	−968
36.2210	1.8265	9,778,155	−876
35.5975	1.8267	9,777,306	−1305
36.5426	1.8269	9,777,675	−1009
36.3575	1.8285	9,778,925	−789
36.0262	1.8325	9,778,246	−887
36.4312	1.8367	9,778,834	−955
36.8175	1.8372	9,776,644	−1085
36.1833	1.8418	9,778,285	−861

Continued

35.5670	1.8467	9,777,344	−1256
36.6432	1.8506	9,776,819	−1041
36.7357	1.8516	9,776,753	−1147
36.5938	1.8532	9,777,227	−1065
36.4949	1.8540	9,778,866	−906
36.6881	1.8552	9,776,966	−1099
35.8275	1.8661	9,777,682	−910
36.1554	1.8770	9,778,365	−824
36.8417	1.8798	9,776,572	−1103
36.0171	1.8812	9,778,293	−850
35.5518	1.8937	9,777,438	−1232
36.4958	1.8983	9,778,978	−810
35.8518	1.9032	9,777,848	−860
36.0449	1.9120	9,778,308	−858
36.1365	1.9149	9,778,442	−785
36.0054	1.9174	9,778,332	−873
36.8632	1.9232	9,776,575	−1128
36.0952	1.9275	9,778,464	−773
35.8779	1.9311	9,778,000	−827
35.5303	1.9326	9,777,520	−1205
35.6966	1.9329	9,777,456	−1011
36.5101	1.9336	9,779,026	−765
36.0269	1.9490	9,778,320	−897
36.0691	1.9491	9,778,351	−892
36.0197	1.9544	9,778,283	−913
35.9049	1.9582	9,778,156	−788
36.8353	1.9584	9,776,647	−1116
35.5277	1.9642	9,777,573	−1216
36.5154	1.9652	9,778,985	−801
35.6777	1.9730	9,777,450	−1056
36.7975	1.9801	9,776,603	−1086
35.6418	1.9803	9,777,474	−1122
35.7891	1.9900	9,777,609	−862
36.0001	1.9933	9,776,212	−945

Continued

35.9355	1.9934	9,778,153	−886
36.0343	1.9947	9,778,276	−935
35.6070	1.9985	9,777,497	−1189
35.9669	1.9996	9,778,176	−938
35.8322	2.0044	9,777,834	−796
36.0604	2.0091	9,778,318	−942
35.9221	2.0115	9,778,068	−904
35.7631	2.0118	9,777,493	−884
35.5251	2.0139	9,777,587	−1248
35.9718	2.0146	9,777,567	−945
35.8673	2.0152	9,778,042	−758
35.5601	2.0193	9,777,497	−1302
36.7867	2.0198	9,776,642	−1033
35.7254	2.0209	9,777,434	−925
35.9188	2.0318	9,777,350	−1019
35.8907	2.0441	9,777,957	−931
35.4928	2.0456	9,777,657	−1118
36.0531	2.0498	9,778,271	−980
36.7732	2.0532	9,776,643	−1000
35.4263	2.0593	9,777,757	−1186
36.0810	2.0734	9,778,312	−959
35.4515	2.0791	9,777,782	−1135
35.8575	2.0812	9,777,949	−959
36.0219	2.0863	9,778,247	−952
35.4830	2.0927	9,777,768	−1100
35.3859	2.0928	9,777,709	−1206
36.7668	2.1039	9,776,739	−959
35.8261	2.1165	9,777,923	−1011
36.1034	2.1177	9,778,436	−866
35.9905	2.1180	9,778,130	−1004
35.3626	2.1290	9,777,717	−1204
35.4983	2.1378	9,777,860	−1091
36.1241	2.1404	9,778,485	−847
35.5466	2.1414	9,777,754	−1100

Continued

36.7623	2.1446	9,776,709	−908
36.1178	2.1530	9,778,500	−853
35.5711	2.1549	9,777,750	−1030
35.7966	2.1581	9,777,925	−1036
35.9798	2.1650	9,778,128	−1014
35.6062	2.1684	9,777,664	−980
35.3384	2.1697	9,777,679	−1203
35.5415	2.1775	9,777,816	−1044
36.7613	2.1807	9,776,929	−860
35.6376	2.1846	9,777,501	−906
36.1106	2.1865	9778,478	−875
35.6739	2.1870	9,778,029	−932
35.6646	2.1918	9,777,763	−898
35.7751	2.1952	9,777,830	−1133
35.7032	2.1989	9,777,884	−918
36.2719	2.2014	9,778,863	−736
36.5744	2.2021	9,778,987	−817
35.9556	2.2057	9,778,122	−1048
36.7613	2.2060	9,776,958	−830
35.5442	2.2083	9,777,834	−1913
36.6292	2.2104	9,778,631	−728
35.3457	2.2149	9,777,815	−1147
35.7338	2.2161	9,777,798	−1114
36.5035	2.2167	9,778,930	−907
36.1078	2.2209	9,778,530	−829
35.7554	2.2241	9,777,787	−1191
36.4360	2.2275	9,778,457	−766
36.6956	2.2340	9,778,467	−751
36.7576	2.2395	9,776,994	−779
35.9243	2.2410	9,778,090	−1085
36.1231	2.2453	9,778,520	−798
35.5551	2.2471	9,777,822	−980
36.2805	2.2500	9,778,301	−760
36.3956	2.2501	9,777,438	−776

Continued

35.5290	2.2535	9,777,873	−993
36.3470	2.2536	9,776,942	−842
35.3350	2.2565	9,777,873	−1129
36.1671	2.2580	9,778,544	−860
35.7339	2.2585	9,777,797	−1201
36.2184	2.2590	9,778,476	−823
35.8983	2.2736	9,778,034	−1137
35.5686	2.2832	9,777,831	−955
36.7207	2.2892	9,776,865	−685
35.3206	2.2918	9,777,861	−1141
35.9675	2.2922	9,778,339	−916
35.7115	2.2965	9,777,837	−1159
36.6740	2.2994	9,778,411	−579
35.5139	2.3014	9,777,952	−977
36.0097	2.3031	9,778,343	−917
36.0592	2.3131	9,778,371	−903
35.5876	2.3203	9,777,830	−896
35.8723	2.3206	9,778,078	−1138
35.6891	2.3309	9,777,911	−1056
35.2947	2.3325	9,777,865	−1106
35.4995	2.3394	9,778,022	−957
35.8392	2.3460	9,777,968	−1159
36.0807	2.3493	9,778,436	−833
35.6218	2.3518	9,778,019	−810
35.6640	2.3662	9,778,132	−818
36.6064	2.3783	9,778,774	−688
35.8078	2.3786	9,777,989	−1158
35.4834	2.3792	9,777,697	−909
35.6982	2.3815	9,777,933	−1075
35.6533	2.3852	9,778,151	−774
35.2947	2.3886	9,777,930	−1104
35.7647	2.3904	9,777,918	−1184
36.1095	2.3937	9,778,526	−798
35.7243	2.3959	9,777,908	−1132

Continued

35.6856	2.3960	9,777,991	−987
36.5516	2.4028	9,778,919	−766
36.1422	2.4034	9,778,671	−785
36.8598	2.4042	9,778,112	−752
36.6171	2.4110	9,776,964	−710
35.4422	2.4118	9,778,106	−969
35.3020	2.4265	9,777,960	−1112
36.8463	2.4431	9,778,206	−720
35.3838	2.4463	9,778,134	−1025
35.6588	2.4512	9,778,141	−791
36.1622	2.4579	9,778,717	−743
36.8273	2.4774	9,778,311	−706
35.2949	2.4790	9,777,976	−1104
35.3291	2.4807	9,777,962	−1159
36.1822	2.4869	9,778,726	−746
35.6616	2.4991	9,778,133	−842
36.5298	2.5067	9,778,359	−711
36.8084	2.5171	9,778,394	−692
35.2716	2.5197	9,777,990	−1006
36.6951	2.5242	9,778,881	−821
36.7706	2.5469	9,778,473	−668
36.1983	2.5475	9,778,712	−779
35.6590	2.5479	9,778,231	−768
35.2321	2.5496	9,777,985	−1017
36.0964	2.5506	9,778,698	−804
35.2582	2.5586	9,778,037	−1019
36.7337	2.5713	9,778,422	−696
35.1926	2.5741	9,776,814	−1084
36.4951	2.5795	9,778,055	633
36.4384	2.5818	9,779,206	−487
36.5800	2.5854	9,778,765	−901
36.7076	2.5866	9,778,699	−755
36.1875	2.5891	9,778,708	−810
35.6591	2.5958	9,778,288	−710

Continued

36.6986	2.6037	9,778,895	−803
35.2538	2.6065	9,778,082	−993
35.3032	2.6146	9,778,085	−1091
35.3536	2.6244	9,778,317	−927
36.0346	2.6252	9,778,148	−542
35.8380	2.6306	9,778,753	−587
35.9027	2.6350	9,778,634	−482
35.9665	2.6367	9,778,635	−441
35.4039	2.6370	9,778,377	−834
35.6493	2.6401	9,778,380	−614
36.5790	2.6415	9,778,888	−813
36.2027	2.6416	9,778,747	−799
36.6967	2.6435	9,778,957	−739
35.4507	2.6468	9,778,302	−786
35.2494	2.6499	9,778,117	−974
35.5001	2.6567	9,778,204	−758
35.5469	2.6656	9777,972	−716
36.1514	2.6723	9,778,703	−831
35.5990	2.6727	9,778,215	−638
36.6958	2.6751	9,778,969	−740
35.6458	2.6772	9,778,433	−592
35.7878	2.6787	9,778,550	−747
35.6997	2.6789	9,778,438	−730
36.2045	2.6896	9,778,757	−814
35.2368	2.6897	9,778,128	−970
36.6018	2.6937	9,779,175	−560
36.3745	2.7087	9,778,955	−440
36.6885	2.7135	9,778,942	−738
36.4366	2.7160	9,779,214	−496
36.7002	2.7186	9,779,016	−703
35.6513	2.7278	9,778,513	−562
35.2360	2.7295	9,778,175	−935
36.2036	2.7303	9,778,766	−829
36.7217	2.7593	9,779,040	−638

Continued

35.6559	2.7693	9,778,626	−525
36.1954	2.7755	9,778,812	−818
35.2316	2.7774	9,778,209	−926
35.1804	2.7947	9,778,083	−1016
36.7054	2.8008	9,778,975	−752
36.3942	2.8038	9,779,120	−586
36.1576	2.8089	9,778,670	−749
35.6452	2.8145	9,778,686	−536
35.2434	2.8299	9,778,272	−910
35.2102	2.8390	9,778,221	−945
36.7044	2.8460	9,779,105	−626
35.6210	2.8490	9,778,609	−558
36.1072	2.8496	9,779,005	−653
36.0361	2.8594	9,779,014	−532
35.2480	2.8832	9,778,342	−891
35.2480	2.8832	9,778,335	−895
36.0918	2.8857	9,778,987	−709
36.6837	2.8867	9,779,141	−593
35.6139	2.8960	9,778,703	−586
36.5209	2.8972	9,779,129	−607
36.0279	2.8992	9,778,974	−634
36.6450	2.8993	9,778,996	−739
36.5704	2.9045	9,779,189	−547
36.7160	2.9075	9,779,151	−524
36.3911	2.9280	9,778,687	−496
35.2688	2.9329	9,778,369	−873
36.0864	2.9355	9,778,995	−731
35.6140	2.9493	9,778,756	−589
36.7321	2.9555	9,778,950	−481
35.3003	2.9590	9,778,360	−924
36.0710	2.9671	9,779,030	−682
36.1052	2.9871	9,778,963	−770
36.7581	2.9899	9,778,885	−436
36.0431	2.9933	9,778,979	−696

Continued

35.5498	3.1056	9,778,825	−649
35.5048	3.0829	9,778,779	−674
35.4588	3.8581	9,778,664	−763
35.4119	3.0320	9,778,713	−669
35.3606	3.0023	9778,418	−919
35.7524	3.1032	9,778,617	−879
35.7664	3.0780	9,778,658	−798
35.8298	3.0717	9778,707	−735
35.8703	3.0609	9,776,786	−794
35.9180	3.0556	9,778,760	−835
35.9612	3.0375	9,778,858	−764
35.9961	3.0132	9,778,056	−789
35.6399	3.1003	9,778,751	−743
35.6120	3.1030	9,778,852	−616
36.3940	3.0290	9,779,032	−715
36.3948	3.0725	9,779,024	−728
36.1232	3.0025	9,778,943	−802
36.7854	3.0212	9,779,039	−454
36.8007	3.0501	9,779,064	−431
36.8475	3.0683	9,779,150	−432
36.8835	3.0973	9,779,155	−431
36.8988	3.0810	9,779,068	−432
36.9267	3.0448	9,779,019	−480